High-Performance Megahertz Wireless Power Transfer: Topologies, Modeling, and Design

Ming Liu, Huang Zhang, Yaoxia Shao, Jibin Song, Chengbin Ma

I. Background and History

At present, mobile energy storage technology (mainly batteries), is still far from satisfactory. For instance, the specific energy of gasoline (∼12,432Wh/kg) is hundreds of times that of a mass-market battery (20-200Wh/kg) [1]. Quite unlike the computational power predicted by Moore's law, the improvement in battery energy density is much slower, basically following a linear trend [2]. In addition to the energy density, battery reliability, weight and cost are also major impediments to the widespread use of electronic devices (e.g., cellphones, wearable devices, medical implants) and electric vehicles [3]–[5]. Charging in a wireless manner is especially expected to significantly enhance the convenience and frequency of charging, and thus potentially be able to

- prolong battery cycle life;
- allow smaller embedded batteries;
- enable easier battery management;
- achieve non-contacting safer charging.

The wireless charging, or wireless power transfer (WPT), provides an important and viable solution without requiring dramatic advances in today's battery technology.

The idea of wireless transfer of electrical energy has been actually known for a long time. Nikola Tesla proposed a "world system" for "the transmission of electrical energy without wires" in 1904 [6]. So far, multiple WPT technologies have been developed and verified, such as inductive coupling, capacitive coupling, microwave and laser radiation. Microwave and laser radiation use far field to wirelessly transfer electric power over meters, or even hundreds of meters [7], [8]. Efforts are required to design a proper antenna array to shape the radiation beam to ensure a high efficiency power transmission. This focused beam usually needs a large size antenna array. High power microwave/laser power sources are also expensive. On the other hand, both inductive coupling and capacitive coupling use near field. The capacitive coupling can transfer power through high-frequency electric fields with negligible eddy-current loss [9]. Meanwhile, its transfer distance and power density are usually lower than

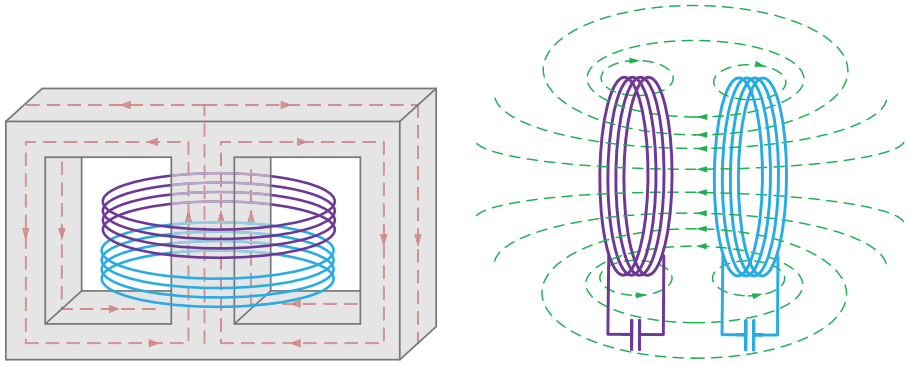

(a) (b)

Fig. 1. Examples of power transfer via inductive coupling. a) Electric transformer. b) Resonating coils.

those of the WPT through the inductive coupling [10]. As shown in Fig. 1 (a), an electrical transformer is a prime example of the power transfer through the inductive coupling. Unlike the transformer, the two coils in Fig. 1 (b) are specially designed with the same resonance frequency, which improves the power transfer distance [11]. Most of commercialized WPT systems use the near-field magnetic resonance coupling and operate in kHz band, such as at several hundreds kHz (typically low and medium-power charging) and 85 kHz (typically high-power charging) [12]–[16]. It is largely because of the availability of the state-of-art power electronic devices for kHz electric power conversion and easiness to design and analyze the circuits at kHz [17]–[19]. On the other hand, the kHz operation requires large-size coils and ferrite materials to achieve a sufficient power transfer distance [20], [21]. It may not be always favorable, especially in terms of the spatial freedom, efficiency, cost, and reliability. Note that the ferrite materials also have other practical benefits in real applications, such as providing better copper utilization and shielding of other electronics.

WPT operating at a higher frequency, such as 6.78 MHz, is now being widely considered as a promising candidate technology for the mid-range transfer of a medium amount of power [22]. Physically, higher operating frequencies improve the spatial freedom of power transfer, and also enable developing more compact and lighter WPT systems [23]. In principle, the MHz WPT does not necessarily require ferrite materials for the power transfer, which facilitates a lightweight design. Meanwhile, the ferrite materials may be needed for the shielding purposes. Thanks to the improved spatial freedom, MHz WPT is particularly effective to charge multiple receivers (e.g., cellphones, smartwatches, and earbuds) at the same time, namely multiple-receiver WPT systems. In such cases, the receiving devices can have very different sizes, positions and orientations, load characteristics, power requirements, etc. The 6.78 MHz is the lowest frequency in the globally recognized ISM (industrial, scientific, and medical) bands. It is the only frequency currently recommended by ITU-R (International Telecommunication Union Radiocommunication Sector) for consumer device WPT because it has minimal or non-existent impact to other licensed bands [24]. For other higher operating frequencies at the ISM bands, such as 13.56 MHz or 27.12 MHz, they further improves spatial freedom, but increases switching loss and driving loss, and presents challenges for circuit design (e.g., PCB layout and component selection) and coupling coil design (e.g., low self-resistance).

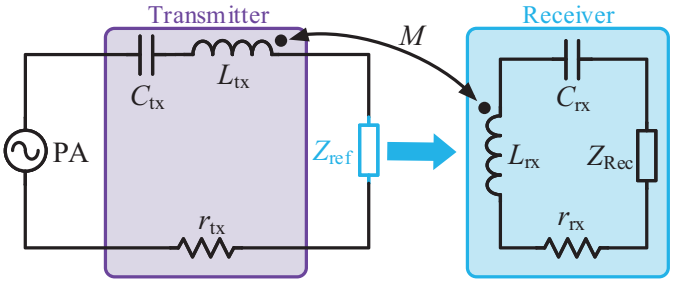

Fig. 2. An equivalent circuit model of a WPT system using the magnetic resonance coupling.

Figure 2 shows a general circuit model of a magnetic resonance based WPT system. Assuming resonance at the same operating frequency ω in both transmitter and receiver,

$$j\omega L_{tx} + \frac{1}{j\omega C_{tx}} = 0 \text{ and } j\omega L_{rx} + \frac{1}{j\omega C_{rx}} = 0, \tag{1}$$

then the reflected impedance Z_{ref}, i.e., the loading effect of the receiver on the transmitter can be derived as [25]

$$Z_{ref} = \frac{\omega^2 M^2}{r_{rx} + Z_{rec}}, \tag{2}$$

where L, C, r with different subscripts (tx and rx) represent the coil inductance, compensation capacitance, and self-resistance of a corresponding coil; M is the coil mutual inductance, and Z_{rec} is the equivalent impedance seen by the receiving coil, namely the input impedance of the rectifier in most cases. Note that

$$M = k\sqrt{L_{tx}L_{rx}}, \tag{3}$$

where k is the mutual inductance coefficient. To achieve high power transfer efficiency and capability, it is straightforward that a reasonable large Z_{ref} is expected. With a higher operating frequency ω, a longer transfer distance (i.e., a smaller M) can be achieved when maintaining the same power transfer capability, namely the same Z_{ref}. When the operating frequency ω is low (such as at kHz), small r_{rx} and Z_{rec} must be achieved for a longer transfer distance, which is challenging in actual design. Meanwhile, with the same small M, increasing ω to the MHz can significantly lower the difficulty in the design of the receiving side, and thus release additional design freedom to further improve the power transfer distance and capability.

The main differences between the MHz and kHz WPT can be summarized as follows:

- The frequency band of kHz WPT covers from tens of kHz to hundreds of kHz, e.g., 20 kHz or 85 kHz for EV charging, and 100–200 kHz for mobile device charging, while the frequency band of MHz WPT is within the ISM band, such as at 6.78 MHz or 13.56 MHz, as mentioned above.
- The MHz WPT provides the improved spatial freedom for the power transfer, namely the longer transfer distance and higher tolerance to the coil misalignment. This advantage is particularly useful to simultaneously charge multiple different receiving devices in a flexible manner, i.e., multiple-receiver WPT systems.
- The kHz WPT usually requires the ferrite materials to enhance the coupling between transmitting and receiving

coils. Meanwhile, in MHz WPT the ferrite materials are principally not required for the power transfer, which facilitates compact and lightweight designs. The ferrite materials may be necessary to provide shielding of other electronics in both the kHz and MHz WPT systems.

- Due to the high switching frequency, the MHz WPT faces the challenge of Electromagnetic Interference (EMI) problem. Both conducted emission (<30 MHz) and radiated emission (>30 MHz) testing are required during the EMI testing in MHz WPT application, while radiated emission test is not necessary in most kHz WPT systems.
- The kHz WPT can achieve high efficiency under a medium or strong coupling due to its low conduction and switching losses. Meanwhile, with loosely coupled coils the MHz WPT systems can achieve higher efficiency than that of the kHz WPT. Their high operating frequencies help lower difficulty in designing the receiving side and thus release additional design freedom when the magnetic coupling is weak.
- The coupling coils of the kHz WPT systems are usually built by Litz wires, which causes a higher cost than the printed-circuit-board (PCB) coils used in the MHz WPT systems. Meanwhile, the high-frequency components required in the MHz WPT systems, such as the switches and driving circuits, are more expensive than those used in the kHz WPT systems. Generally, the circuit complexity and cost of the kHz and MHz WPT systems are comparable.
- The high operating frequency of the MHz WPT increases the system design complexity. The load dependent output characteristics of the single-switch power amplifiers (PAs), as explained in Section II, also add additional complexity in the power/voltage regulation of the MHz WPT systems.

The unique technical challenges of the MHz WPT, due to its high-frequency operation, are then briefly as follows,

- More obvious influence of device parasitic parameters and thus non-negligible reactance [26];
- Potentially higher switching and conduction loss and thus lower system efficiency;
- More challenging Electromagnetic Interference (EMI) problem [27], [28];
- Robustness against varying operation conditions, such as uncertainties in the load and relative position of the coils.

Thus, due to the high-frequency operation, circuit-level complexity and multiple objectives in real MHz WPT systems, system-level analysis and design are especially important to achieve high performance (e.g., high-efficiency, low-noise, and robust) of a final MHz WPT system. As discussed in the following sections, major power conversion

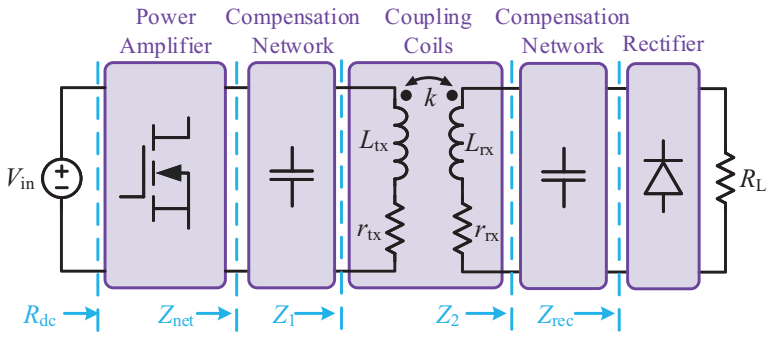

Fig. 3. A general configuration of WPT systems.

topologies are first reviewed and compared; then a systematic scheme is explained to model and design a complete MHz WPT system, taking a Class E^2 topology as an example [29]; the scheme is further extended to a multiple-receiver MHz WPT system, in which robustness of operation is particulary addressed. The developed modeling and design scheme is based on the impedance analysis of each component, from final load, rectifier, coupling coils, to the PA. Therefore, this scheme, i.e., the design concept, is general for MHz WPT systems using other representative circuit topologies. Finally, two actual user cases, namely a single-receiver system and a multiple-receiver system that both operate at 6.78 MHz, are taken as the examples to demonstrate the implementation and results according to the above design scheme.

II. Power Conversion Topologies

Generally, a WPT system consists of three stages for dc-ac (power amplifier, namely PA), ac-ac (coupling coils), and ac-dc (rectifier) power conversions, as shown in Fig. 3. For the coupling coils, i.e., ac-ac conversion, there are mainly four basic topologies to compensate the coil inductance for resonance, i.e., series-series (SS), series-parallel (SP), parallel-parallel (PP), and parallel-series (PS) compensations [see Fig. 4] [25], [30]. The SS compensation is the most widely used in the MHz WPT because this topology is

- straightforward to achieve the full resonance of the coupling coils [refer to (1)];
- capable to provide a pure resistive load to the PA with any mutual inductance coefficient of the coupling coils and final load, when the two coupling coils are both fully resonant [31];
- suitable for the following current-driven circuits, such as the current-driven Class E rectifiers.

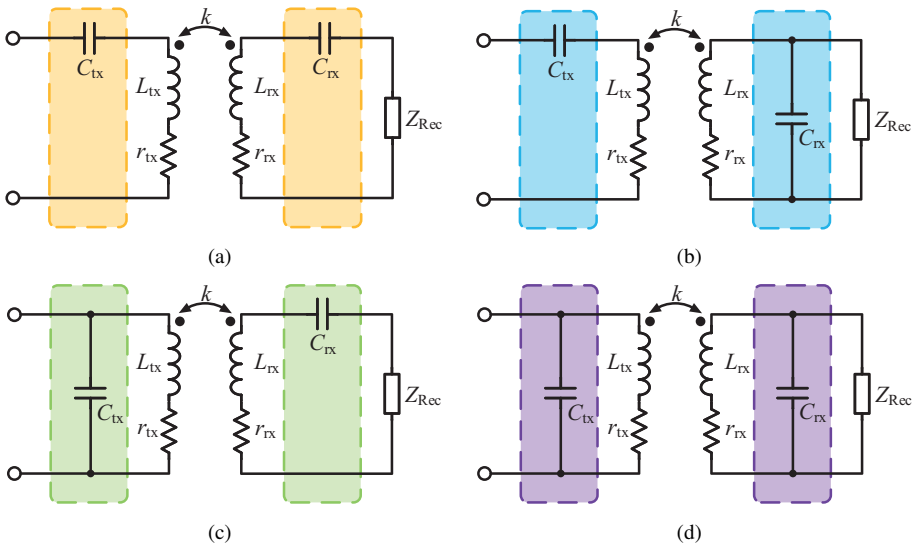

Fig. 4. Four basic compensation topologies. a) SS; b) SP; c) PS; d) PP.

For the dc-ac and ac-dc conversions, the full-bridge (i.e., voltage-mode Class D), Class E, and Class EF_2 topologies have been proposed for the MHz WPT, as shown in Fig. 5.

1) *Full-bridge topology*: The full-bridge PAs/rectifiers shown in Fig. 5(a) and (d) are popular in classical power electronics due to its simplicity, low switch stress, and high robustness [32]. For practical WPT systems,

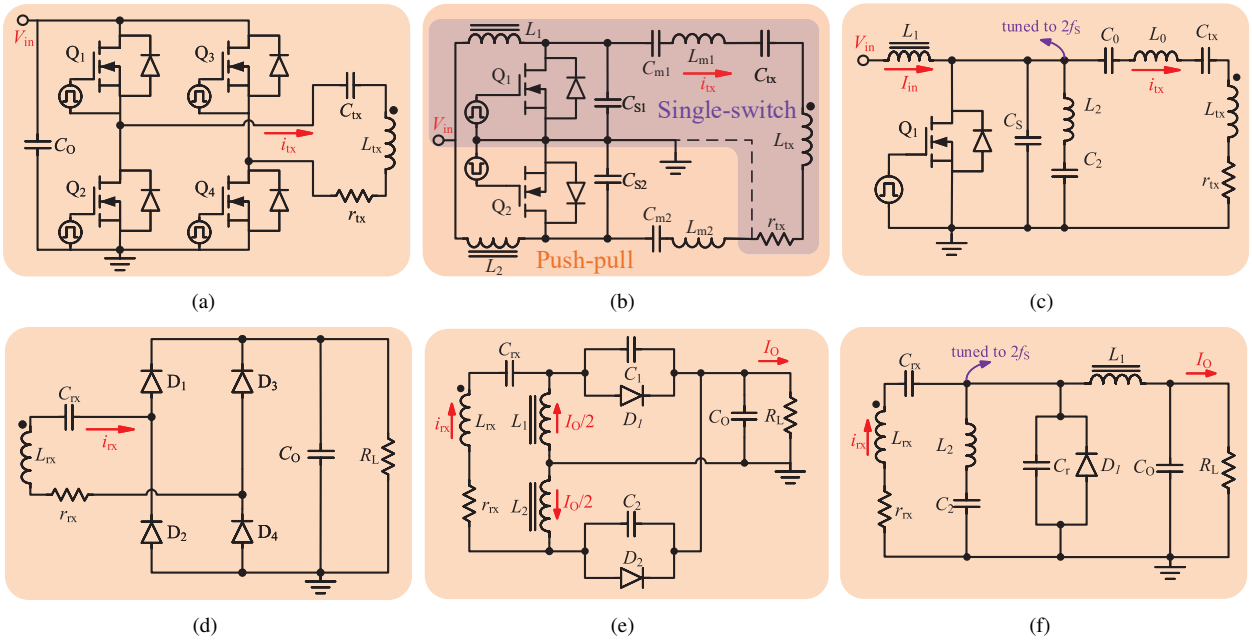

Fig. 5. Power conversion topologies for MHz WPT. (a) Full-bridge PA; (b) Push-pull/single-switch Class E PAs; (c) Class EF_2 PA; (d) Full-bridge rectifier; (e) Full-wave Class E rectifier; (f) Class EF_2 rectifier.

the robustness is important because the changes in relative position of the coupling coils and final load usually occur. Meanwhile, because of its square-wave operation, the total harmonic distortion (THD) of the output/input voltages are high in the full-bridge PAs/rectifiers [33]. This disadvantage significantly affects the Electromagnetic Interference (EMI) performance of the MHz WPT systems. Besides, the required dead time makes it challenging to drive the full-bridge PA when operating at MHz [34].

2) *Class-E topology*: The Class E PAs/rectifiers were proposed for high frequency applications [35], [36]. The single-ended topology makes the Class E PA easier to drive at MHz. The Class E topology, either for PA or rectifier, is a promising candidate for high switching frequencies, thanks to its simple topology and soft-switching property, i.e., zero-voltage switching (ZVS) and zero-voltage-derivative switching (ZVDS) [37]. At the same time, this topology is also known to be sensitive to its loading condition, which requires a system-level design to improve the robustness of the entire WPT system [38]. Corresponding to the full-bridge PA, Fig. 5(b) shows a push-pull Class E PA. The two gate driving signals are in 180° out of phase. This push-pull topology can achieve a higher power level and lower harmonic contents than those of the classical single-switch Class E PA [39], [40]. Due to the 180° out-of-phase driving, each of its branches provides half waveform of the output voltage (V_{out}) and half output power (P_{out}). Thus, the below relationship exists,

$$P_{out} = \frac{{V_{out}}^2}{R_{load}},\ P_1 = \frac{{V_1}^2}{R_1} = \frac{{V_{out}}^2}{4R_1} = \frac{1}{2}P_{out} \Rightarrow R_1 = \frac{1}{2}R_{load}, \tag{4}$$

where P_1, V_1 and R_1 is the output power, output voltage, and equivalent load of a branch; R_{load} is the actual load of the PA. Therefore, each branch sees only half of the load impedance, which improves the robustness against the load variation. Similarly, a current-driven full-wave Class E rectifier is shown in Fig. 5(e) [41].

Table I . Comparison of Power Conversion Topologies

Topology	V_{peak}/V_{dc}	I_{peak}/I_{dc}	Voltage THD (%)	No. of switches	No. of RF inductors	No. of RF chokes	Robustness	Features
Full bridge PA/Rectifier (D=0.5)	1	1.57	41.6	4	0	0	High	- Low switch stress - Fixed voltage ratio - 50% duty cycle
Class E Push-pull PA /Full-wave Rectifier (D=0.5)	3.56	1.43	13.46	2	2 (PA) 0 (Rectifer)	2	Low	- Single-ended drive - Low THD - 50% duty cycle
Class EF_2 PA/Rectifier (D=0.375)	2.31	3.26	45.38	1	2 (PA) 1 (Rectifer)	1	Medium	- Single-ended drive - Low voltage stress

Thanks to the current-driven operation, this rectifier can be used in WPT systems with SS or PS compensation. Inductors L_1 and L_2 are RF choke inductors, which are more compact and efficient than finite inductors. The Class E rectifier provides a new degree of freedom in design, i.e., the capacitances of the shunt capacitors C_1 and C_2, to

- tune the voltage ratio of input ac voltage to output dc voltage;
- design the rectifier input impedance;
- reduce the harmonic contents.

The full-wave/push-pull topologies especially have a superior EMI performance, i.e., low harmonic contents, because the output (for the PA)/input (for the rectifier) current and voltage are both close to sinusoidal [33]. Meanwhile, the classical single-switch topologies are also useful because of their simplicity and compactness [38].

3) *Class-EF_2 topology*: The peak voltages across switches of the Class E topology are about 3 to 4 times of the dc input/output voltage, namely high voltage stresses [37]. As shown in Fig. 5(c) and (f), the Class EF_2 topology has been discussed to reduce the voltage stresses through adding L_2C_2 network [42]. This network is tuned to match the second harmonic of the switching frequency. Thus, the switch drain voltage does not contain the second-harmonic component because the harmonic at this order is "shorted" by the series L_2C_2 network. This helps reduce the voltage stresses of the switches and improve the robustness. Meanwhile, the ac inductor in the L_2C_2 network enlarges the size and induces additional power loss.

The above three topologies, the full-bridge, push-pull/full-wave Class E, and Class EF_2 ones, are compared in Table I, in terms of voltage stress (V_{peak}/V_{dc}), current stress (I_{peak}/I_{dc}), total harmonic distortion (THD), components count, and robustness. As a summary,

1) The full-bridge PA/rectifier achieve a low switch stress, but with higher harmonic contents. Its high-side driving is also challenging, leading to additional driving loss and cost at MHz.
2) The Class E and EF_2 PAs are both single-ended driven, which is easy to implement at high frequency. But

they have higher switch stress than that of the full-bridge PA. As discussed in the below section, the switch parasitic capacitance can be explicitly reflected during the design of the Class E/EF$_2$ PAs/rectifiers instead of being neglected when designing the full-bridge ones.

- The Class EF$_2$ topology achieves a lower switch voltage stress than that of the Class E topology, thanks to the additional series L_2C_2 network and operation with a duty cycle lower than 50%. Meanwhile, the bulky ac inductor in the L_2C_2 network increases circuit size and power loss. The non 50% duty cycle driving signal is also challenging to generate at high frequencies.
- Thanks to the sinusoidal current and voltage, the push-pull Class E PA and full-wave Class E rectifier achieve lower THD than their full-bridge and Class EF$_2$ counterparts. This is especially helpful for the EMI performance of the MHz WPT systems.

III. System-Level Modeling and Design

As mentioned in Section I, the system-level modeling and design are especially important for the high-frequency MHz WPT systems. In the following two subsections, a high-efficiency single-receiver system is first used as an example to explain the impedance-based design procedures, which are reverse to the path of power transfer (i.e., from the final dc load on the receiving side to the PA on the transmitting side); then this design scheme is extended to a multiple-receiver MHz WPT system, in which not only efficiency, but also robustness and power distribution among the receivers need to be addressed.

A. Single-Receiver MHz WPT Systems

As shown in Fig. 3, a single-receiver system usually consists of a dc power source, a PA, two compensation networks, coupling coils, a rectifier and a dc final load. Here the Class E^2 topology, namely with Class E PA and rectifier, is chosen as an example to facilitate the below explanation of the design procedures. Note that the basic concepts of these procedures are general that can be extended to MHz WPT systems using other circuit topologies.

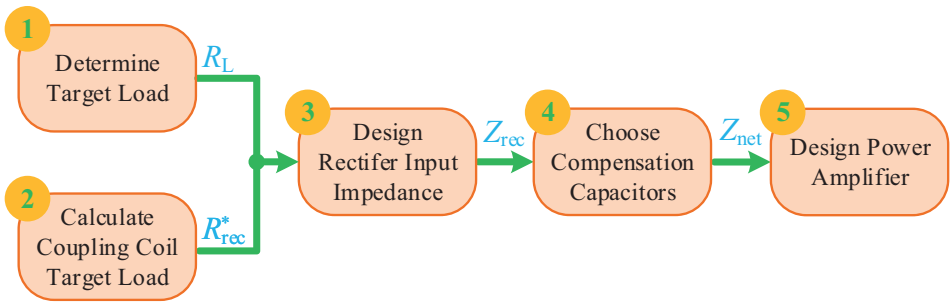

Fig. 6. The system-level design flow for MHz WPT systems.

The flow chart in Fig. 6 summarizes the procedures that implement the system-level modeling and design in a step-by-step manner. Below the label Z_{net} is the PA output impedance; Z_{rec} is the rectifier input impedance; Z_1 and Z_2 are the input impedance and output impedance of the coupling coils; and R_{dc} is the input dc resistance of the entire WPT system [refer to Fig. 3].

1) *Final dc load*: The target final dc load, namely R_L in Fig. 6, should be firstly determined. For instance, lithium-ion batteries are today's most popular loads, largely due to their high energy densities. A typical charging profile of a lithium-ion battery usually consists of two modes, constant current (CC) mode and constant voltage (CV) mode, which can be used to determine the varying range of the final dc load for the system-level design [43]. Fig. 7 shows the charging profile and corresponding charging power and equivalent load of an example lithium-ion battery pack. During the CC mode, charging current maintains constant and battery voltage slowly increases, which leads to a relatively stable equivalent load and high charging power. In the following CV mode, charging voltage maintains constant and charging current rapidly decreases. This corresponds to a significant increase of the equivalent load and low charging power. Therefore, the load variation range can be estimated in advance from the battery charging profile. Practically, optimizing the charging performance is the most important. Thus the value of the target final dc load, when designing the MHz WPT system, should be taken as the equivalent dc load during the CC mode, which is, for example, 30 Ω for a 18V/0.6A battery pack.

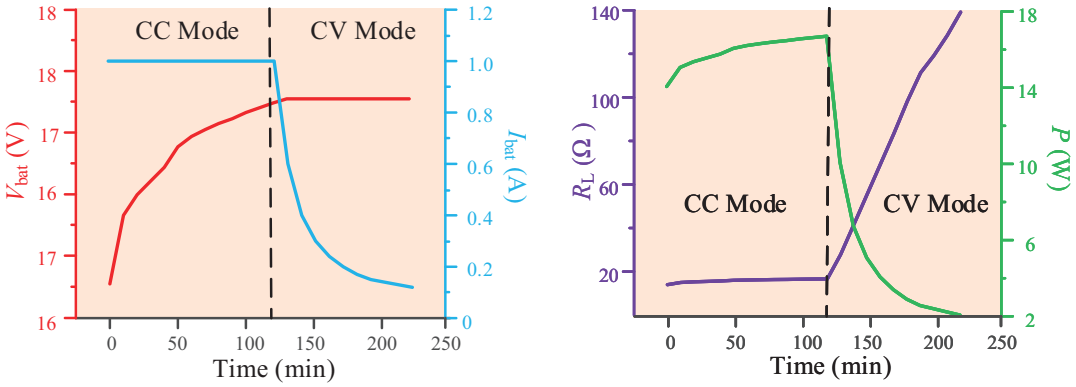

Fig. 7. An example lithium-ion battery pack. (a) Charging current and voltage profiles; (b) Charging power and equivalent load.

2) *Coupling coil target load*: The overall power transfer efficiency is largely influenced by the coupling coils. A target load for the coupling coils, which maximizes the coil-to-coil efficiency, should be calculated to guide the following design of the rectifier input impedance. Fig. 8 shows the circuit model of the coupling coils. The coil-to-coil efficiency is jointly determined by the mutual inductance coefficient k, inductances and equivalent series resistances (ESRs) of the transmitting coil and receiving coil, compensation capacitors, and the load impedance seen by the receiving coil Z_{rec} (i.e., the rectifier input impedance). For a high coil-to-coil efficiency, the receiving side should be designed to achieve full resonance, and an optimal R^*_{rec} can then be analytically derived as [25]:

$$R^*_{rec} = \sqrt{\frac{r_{tx}{r_{rx}}^2 + \omega^2 k^2 L_{tx} L_{rx} r_{rx}}{r_{tx}}} \tag{5}$$

Note that usually the parameters of the coupling coils, r_{tx}, r_{rx}, L_{tx}, and L_{rx}, are pre-determined in a target application. In practice, coupling coils must be placed in the available space, and the transfer distance is

mostly predefined for a specific application. Under the constraints of target mutual inductance coefficient k and the load, the parameters of coupling coils, r_{tx}, r_{rx}, L_{tx}, and L_{rx}, can be achieved by optimizing the shape, turns, trace width/spacing of the coupling coils and considering the required shielding. There are also commercial coil designs recommended by standards organizations [44].

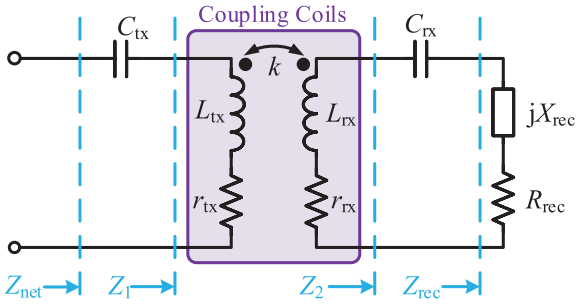

Fig. 8. Circuit model of the coupling coils.

3) *Rectifier input impedance*: For a Class E rectifier, such as the full-wave one in Fig. 5(e), the capacitances of its parallel capacitors, C_1 and C_2, are the parameters to design the rectifier input impedance. For the sake of simplicity and symmetric performance, C_1 and C_2 usually take the same capacitance, C_r here [33]. In terms of design, an important advantage of the Class E topology is that the relationships among its parameters can be analytical derived. As mentioned above,
   a) the rectifier input resistance R_{rec} should be as equal as R^*_{rec} to have a high coil-to-coil efficiency;
   b) the desired duty cycle of the rectifier D^* can be calculated based on the derived relationship between R_{rec} and D [45], [46]. This duty cycle corresponds to a specific value of C_r;
   c) this specific C_r then can be used to calculate the rectifier input reactance X_{rec}, which helps design the compensation capacitor on the receiving side, C_{rx} [refer to Eq. (6)].

   Fig. 9 illustrates the design procedure of the example Class E full-wave rectifier, following the above three steps, a)–c), starting from determining R_{rec}. Note that in order to reduce the harmonic contents caused by the overlapping of the diode conduction, D should be smaller than 0.5, which may compromise the achievable optimal R_{rec}.
4) *Compensation capacitors*: As mentioned in Section II, the SS compensation is widely applied in the WPT systems. Unlike in the kHz WPT systems, where their rectifier input impedances are close to pure resistive, the rectifier input reactances become non-negligible at multi-MHz [47]. As shown in Eq. (6), the design of the compensation capacitors, C_{rx} and C_{tx}, must reflect the nonnegligible rectifier input reactance X_{rec}, especially in order to make the receiving coil fully resonant [45].

$$C_{rx} = \frac{1}{\omega\left(\omega L_{rx} + X_{rec}\right)},\ C_{tx} = \frac{1}{\omega^2 L_{tx}}. \tag{6}$$

5) *PA parameters*: Due to the full resonance on both the transmitting side and receiving side, the PA load

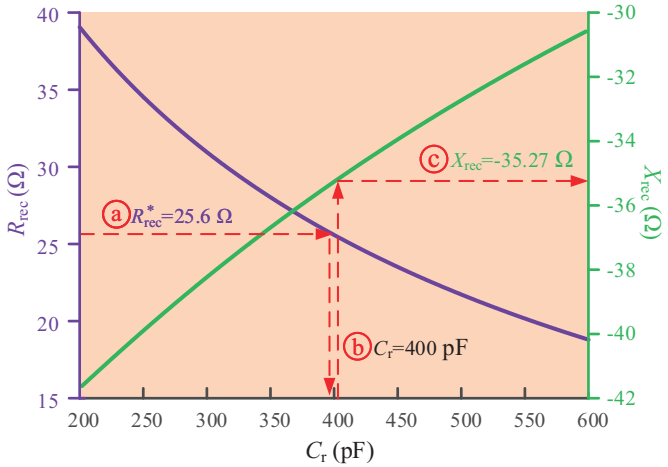

Fig. 9. Design procedure of the Class E rectifier (R_L=30 Ω).

impedance Z_{net} can be derived as [see Fig. 3]

$$Z_{net} = R_{net} = r_{tx} + \frac{\omega^2 k^2 L_{tx} L_{rx}}{r_{rx} + R_{rec}}, \tag{7}$$

which is pure resistive. It is known that based on R_{net}, the parameters of a single-switch Class E PA can be calculated to enable the ZVS operation of the PA, following the Raab's equations [48][see Fig. 5(b)],

$$C_S = \frac{0.1836}{\omega R_{net}}, \; X_{m1} = \omega L_{m1} - \frac{1}{\omega C_{m1}} = 1.1525 R_{net}. \tag{8}$$

Note that L_{m1} should be determined by the loaded qualify factor Q, usually between 2 and 5 [49]. When designing the push-pull Class E PA, a half R_{net} of the PA can be used to determine the parameters $C_{S1,2}$ and $C_{m1,2}$ to achieve the ZVS operation.

The above five impedance-based procedures guide the design of the major components of high-efficiency MHz WPT systems (from the rectifier to the coupling coils and then PA). Each component's optimal parameters are determined by desired loading conditions provided by other components, i.e., a system-level design. As a supplementary discussion, for WPT systems employing the conventional full-bridge rectifier, the design procedures are similar. It is well-known that in a kHz WPT system, the input impedance of the full bridge rectifier is close to pure resistive, and it has a fixed relationship with the load [37],

$$R_{rec} = \frac{8}{\pi^2} R_L. \tag{9}$$

However, when working at MHz, the influence of diode junction capacitors becomes obvious. This causes the rectifier input impedance to no longer be pure resistive, and its reactance changes with load and diode selection [47]. Unlike the Class E rectifier, which has C_r as its design parameter, the full-bridge rectifier lacks freedom to design its input impedance. Thus it is difficult to match the coupling coil target load. Simulation can be performed to obtain the values of R_{rec} and X_{rec} of the full-bridge rectifier, such as using Advanced Design System (ADS) from Keysight

Technologies (i.e., Agilent previously) and Spice models of the diodes [50]. Again, the calculated X_{rec} is useful to determine the compensation capacitor C_{rx}.

B. Extension to Multiple-Receiver MHz WPT Systems

This subsection further extends the above design scheme into a multiple-receiver MHz WPT system. As mentioned in Section I, a unique advantage to increase the operating frequency to several MHz is to improve the spatial freedom of the power transfer, i.e., with a longer transfer distance and a higher tolerance against the coil misalignment. This is especially important for the multiple-receiver WPT systems. In such systems, receivers may have different sizes, positions and orientations, power requirements, and loading characteristics, such as when simultaneously charging a cellphone, smart watch, and ear buds. The possible cross coupling (i.e., non-zero mutual inductances) between the receivers is particularly challenging because it significantly influences the efficiency and power distribution among the receivers [51], [52].

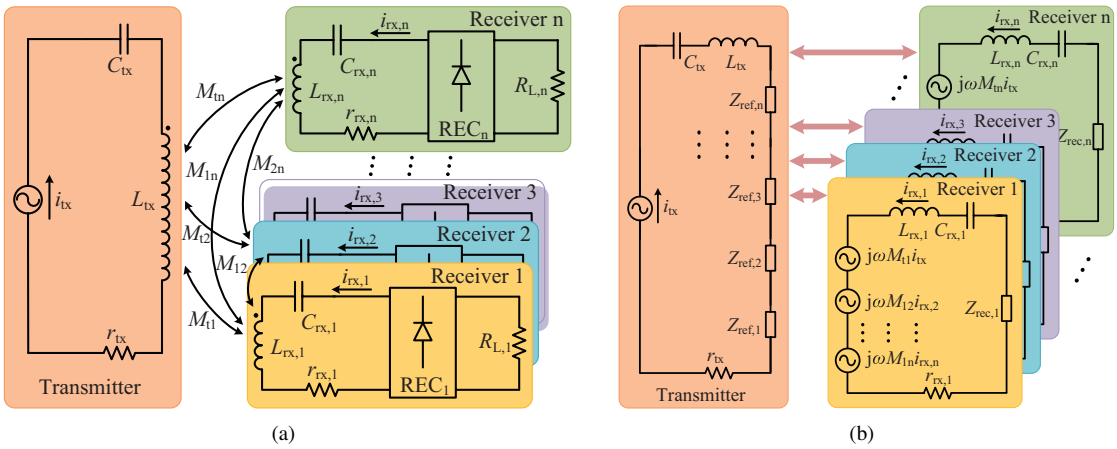

Fig. 10. A typical multiple-receiver WPT system. (a) Circuit model; (b) Equivalent circuit model.

Existing solutions include multiple operating frequencies for different receivers [53]–[55], time division schemes [56], game theory-based active control [57], [58], etc. Note that the narrow industrial-scientific-medical (ISM) band imposes limitation on choosing the available operating frequencies. A fixed frequency, such as 6.78 MHz, is usually preferred, in terms of actual applicability. Implementation of the active control also requires dedicated hardware (such as dc-dc converters) and communication between the transmitting and receiving sides. Instead, here the performance of a multiple-receiver MHz WPT system is optimized through the parameter design to achieve high efficiency and maintain desired power distribution among the receivers. The robustness against the cross coupling is particularly reflected and enhanced during the parameter design [59].

Fig. 10(a) shows the circuit model of a typical multiple-receiver WPT system. The single transmitting coil and n receiving coils are represented by their inductances L_{tx} and $L_{rx,i}$ ($i \in [1, n]$), and ESRs r_{tx} and $r_{rx,i}$. Both the transmitting coil and receiving coils are compensated by series-connected capacitors, C_{tx} and $C_{rx,i}$'s. Here M_{t1}—M_{tn} are the mutual inductances between the transmitting coil and i-th receiving coil; M_{ij}, where $i, j \in [1, n]$, is the mutual inductance between the i-th and the j-th receiving coils. The transmitting coil is assumed to be driven

by a sinusoidal current source, i_{tx}. REC_i and $R_{L,i}$ are the rectifier and dc load of the i-th receiver. The equivalent circuit model of the multiple-receiver WPT system is given in Fig. 10(b). The coupling effects on the receiving side including the cross coupling are represented by the induced voltage sources, and the rectifier input impedances are $Z_{rec,i}$'s. Again, the coupling coils achieve an optimal power transfer efficiency when all the receiving coils are fully resonant. Theoretically, the compensation capacitors $C_{rx,i}$ of the receiving coils can be determined as follows,

$$C_{rx,i} = \frac{1}{\omega \left[\omega L_{rx,i} + X_{rec,i} + \sum\limits_{j=1}^{j=n, j\neq i} \frac{\omega M_{ij} M_{tj} (R_{rec,i} + r_{rx,i})}{M_{ti}(R_{rec,j} + r_{rx,j})} \right]}, \tag{10}$$

where $X_{rec,i}$ is the i-th receiver's input reactance. It can be seen that the optimal $C_{rx,i}$ depends on the cross coupling between the receivers (i.e., M_{ij}'s). However, in actual scenarios, it is almost unavoidable to have uncertainties in the number of the receivers, their relative positions and orientations (i.e., changing M_{ij}'s). A design scheme is particularly expected to enhance the robustness of system performance, in terms of maintaining high efficiency and target power distribution.

It would be ideal to achieve a multiple-receiver WPT system that always provides the required power to an individual receiver. This amount of power should not be affected by the existence of other receivers and the cross coupling, namely decoupled power transfer. Thus, the system design must take into account the uncertainties in the number of receivers and cross coupling between them. As shown in Fig. 10, ideally if the PA always outputs a constant ac current i_{tx} and the cross coupling is negligible, the received power of each receiver is solely determined by its impedance seen on the transmitting side, i.e., its reflected impedance $Z_{ref,i}$ in Fig. 10(b). To achieve this decoupled power transfer, efforts are twofold,

1) *Supporting circuit topology*: This topology should be able to provide a constant PA output current and the required design freedom;
2) *Robust design methodology*: To achieve the decoupled power distribution among the receivers, this methodology must explicitly address the robustness against the uncertainty in the cross coupling and also properly determine the reflected impedances of the receivers.

As shown in the following Fig. 13(a), the Class E^2 topology is again a suitable candidate as the supporting circuit topology. An impedance transformation network (ITN) is added after the classical Class E PA and designed to largely maintain a constant PA output current despite the uncertainties in the number of the receivers and cross coupling, namely a current-mode Class E PA [38]. The parallel capacitors of the Class E rectifiers, $C_{r,i}$'s, rightly provide a degree of freedom to design the reflected impedances of the receivers [45]. In real applications, the wireless charging area is usually limited, such as over a charging mat. Thus the variation range of the cross coupling is predictable according to the maximum/minimum possible distances between the receiving coils. The robust design problem can then be formulated as follows.

- Constant parameters $\mathbf{p}$ (usually pre-determined in an initial design):

$$\mathbf{p} = [\omega,\ L_{tx},\ r_{tx},\ \mathbf{p_1},\ \mathbf{p_2}, \cdots\ \mathbf{p_n}]_{1\times(3+4n)} \text{ and } \mathbf{p_i} = [k_{ti},\ L_{rx,i},\ r_{rx,i},\ R_{L,i}]_{1\times 4}. \tag{11}$$

The above constant parameters include the operating frequency (ω), coil inductances and ESRs ($L_{tx}, L_{rx,i}, r_{tx}, r_{rx,i}$), mutual inductance coefficients between transmitting coil and receiving coils (k_{ti}), and loads of receivers ($R_{L,i}$). Note that k_{ti} and M_{ti} have a relationship defined in (3), and n is the maximum number of receivers.

- Design variables $\mathbf{x}$:

$$\mathbf{x} = [|I_{tx}|,\ C_{r,1},\ C_{r,2}, \dots\ C_{r,n}]_{1\times(1+n)}, \tag{12}$$

where $|I_{tx}|$ is the magnitude of the PA's constant ac output current; again, $C_{r,i}$'s are the capacitances of the rectifier parallel capacitors.

- Objective function and constraints:

$$\begin{aligned} \max_{\mathbf{x}} \quad & \eta_{coil2load}^{nom}(\mathbf{x}), \\ s.t. \quad & \chi(\mathbf{x}) \le \chi^{\max}, \\ & \gamma(\mathbf{x}) \le \gamma^{\max}, \\ & \mathbf{k^{low}} \le \mathbf{k} \le \mathbf{k^{upp}}, \end{aligned} \tag{13}$$

where

$$\chi(\mathbf{x}) = \max_{\mathbf{x}} \left| \frac{\eta_{coil2load,m}(\mathbf{x},\mathbf{k}) - \eta_{coil2load,m}(\mathbf{x},\mathbf{k=0})}{\eta_{coil2load,m}(\mathbf{x},\mathbf{k=0})} \right|, \tag{14}$$

$$\gamma(\mathbf{x}) = \max_{\mathbf{x}} \left| \frac{P_{R_L,i,m}(\mathbf{x},\mathbf{k}) - P^*_{R_L,i}}{P^*_{R_L,i}} \right|, \tag{15}$$

$$\mathbf{k} = \left[k_{12},\ k_{13}, \dots\ k_{ij}, \dots\ k_{(n-1)n}\right]_{1\times C_n^2}. \tag{16}$$

The purpose of the above objective function in (13) is to maximize the total system efficiency from the transmitting coil to the final loads ($\eta_{coil2load}^{nom}$) under a nominal condition, i.e., the condition with negligible cross coupling. The first and second constraints are defined to restrict the maximum deteriorations of the efficiency ($\chi(\mathbf{x})$) and power distribution ($\gamma(\mathbf{x})$) described in (14)(15), respectively, when the cross coupling changes within the range defined by $\mathbf{k^{upp}}$ and $\mathbf{k^{low}}$, namely the last constraint (16). The vector $\mathbf{k}$ represents an array of the mutual inductance coefficients between any two receiving coils (i.e., the cross coupling). In (14)(15), $\eta_{coil2load,m}$ and $P_{R_L,i,m}$ are the system efficiency and load power of the i-th receiver under a specific combination of receivers m ($2^n - 1$ combinations in total). The detailed derivations of efficiency from the transmitting coil to final loads and the load powers can be found in [59]. This nonlinear robust design problem can then be solved, such as through the genetic algorithm (GA) [60], [61].

Therefore, the optimal rectifier parallel capacitors $C_{r,i}$'s can be obtained via the above robust design. After this robust design, the similar procedures, i.e., 3) – 5) in Section III-A, can be applied to determine the other parameters of the multiple-receiver MHz WPT system. The rectifier input impedances under the nominal condition can be calculated based on the optimal $C_{r,i}$; then the compensation capacitors of the coupling coils are determined to enable full resonance on the both receiving side and transmitting side [refer to (6)]; the PA load impedance Z_{net} in (7) varies with different combinations and positions of the receivers, namely the changing $\mathbf{k}$ in (16). Its variation range can then be used to design the ITN that transforms the impedance seen by the classical single-switch Class

Table II. Parameters of Experimental MHz WPT System

Coupling Coils		k	f	r_{tx}	r_{rx}	L_{tx}	L_{rx}	R^*_{rec}
		0.18	6.78 MHz	0.8 Ω	0.8 Ω	3.34 μH	3.34 μH	26.0 Ω
System-level Design (with Full-wave Class E Rectifier)	**Rectifier & Comp.**	D	C_r	Z_{rec}		C_{rx}	C_{tx}	Z_{net}
		0.375	412 pF	28.5-j53.0 Ω		265 pF	165 pF	22.1 Ω
	Class E PA	D	L_1	L_{m1}	C_{m1}	C_{S1}		
		0.5	68 μH	1.47 μH	655 pF	187 pF		
Conventional Design (with Full-Bridge Rectifier)	**Rectifier & Comp.**	D	C_r	Z_{rec}		C_{rx}	C_{tx}	Z_{net}
		0.5		24.3 Ω		165 pF	165 pF	26.1 Ω
	Class E PA	D	L_1	L_{m1}	C_{m1}	C_{S1}		
		0.5	68 μH	1.47 μH	726 pF	165 pF		

E PA to achieve high-efficiency operation and the constant output current, namely a current-mode Class E PA [38]. Thus the classical Class E PA itself can be simply designed based on its nominal load R^*_{net} [refer to (8)].

IV. User Cases

Two actual user cases, namely a single-receiver system and a multiple-receiver system that both operate at 6.78 MHz, are taken as the examples to demonstrate the implementation and results according to the above design procedures in Section III. The experimental single-receiver system in Fig. 11 consists of two coils with a dimension of 10×10 cm^2 and a distance of 3.3 cm (k=0.18). The final dc-dc system efficiency is 87%, but without the need of ferrite materials. Meanwhile, the multiple-receiver system in Fig. 13(a) contains maximum three receiving coils with a diameter of 7.2 cm. The diameter of the transmitting coil is 20 cm, and the transfer distance is 2.2 cm. The experimental results show that the designed multiple-receiver system can maintain stable power distribution and high efficiency despite variations in number and positions of the receiving coils.

A. A Single-Receiver MHz WPT System

The 6.78 MHz single-receiver system in Fig. 11 employs the single-switch Class E PA and the full-wave Class E rectifier, i.e., a Class E^2 system. This MHz WPT system is optimally designed according to the system level design procedures explained in Section III-A. As a comparison, a similar system is designed but using a full-bridge rectifier and the assumed pure resistive input impedance of the rectifier in (9). This conventional design is popular when designing kHz WPT systems. The parameters of the two designs are listed in Table II. Note that C_r and C_{S1} absorb parasitic capacitances of the rectifying diodes and PA switch. The rectifier input powers of the two systems are both around 10 W.

Experimental results are given in Fig. 12(a)-(c). Applying the design procedures explained in Section III-A, a well-designed full-wave Class E rectifier demonstrates superior performance, in terms of both efficiency and EMI suppression. Especially thanks to the design freedom provided by the Class E rectifier topology, the coil-to-coil efficiency and rectifier efficiency can be improved at the same time, which helps to achieve a high dc-to-dc system

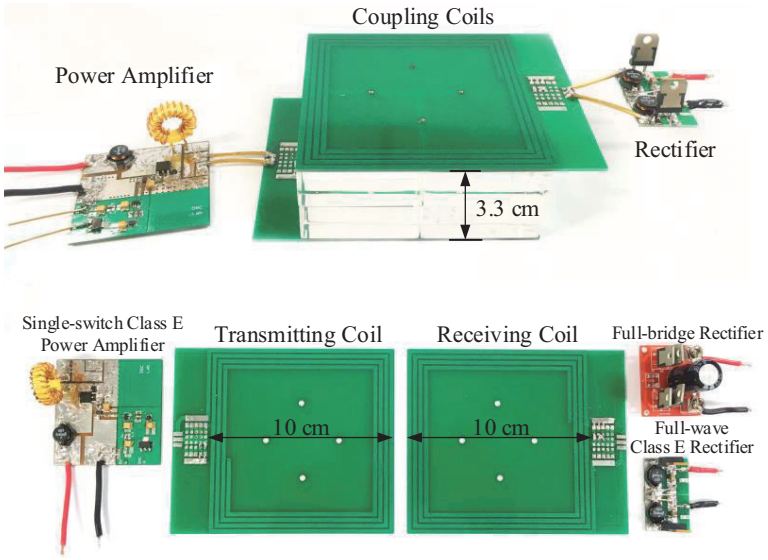

Fig. 11. Experimental setup of a single-receiver WPT system.

efficiency of 87%. Compared to the full-bridge rectifier, the input voltage THD of the full-wave Class E rectifier is largely reduced by 64.9%. The EMI performance of the rectifier is particularly important because the rectifier is usually located inside a receiving device, such as a cellphone.

B. A Multiple-Receiver MHz WPT System

The experimental setup of the three-receiver WPT system in Fig. 13(a) employs a current-mode Class E PA, which combines the single-switch Class E PA and ITN, and three receivers using half-wave Class E rectifiers. The circuit parameters are determined according to robust design described in Section III-B. The target load powers of the three receivers are 10 W ($P_{R_L,1}$), 8 W ($P_{R_L,2}$), and 6 W ($P_{R_L,3}$), respectively. As shown in Fig. 14, the three receivers are first placed with 120° angular position difference. After each 100 s, one of the receivers is removed, and returned later to the same position. It can be seen that the received power of each receiver remains almost constant whenever other receivers join or quit the charging, i.e., decoupled power distribution. The dash lines in

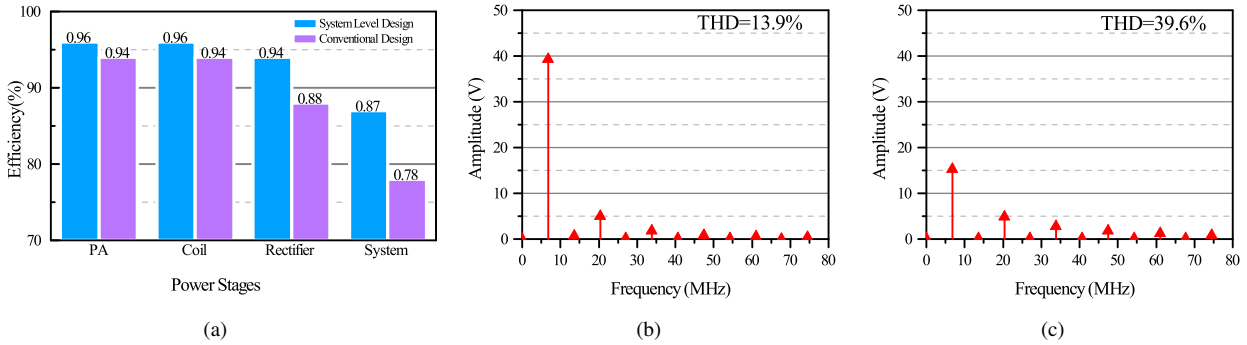

Fig. 12. Experimental results of the single-receiver WPT system. (a) Efficiency breakdown; (b) THD of input voltage of the full-wave Class E rectifier (10 W rectifier input power); (c) THD of input voltage of the full-bridge rectifier (10 W rectifier input power).

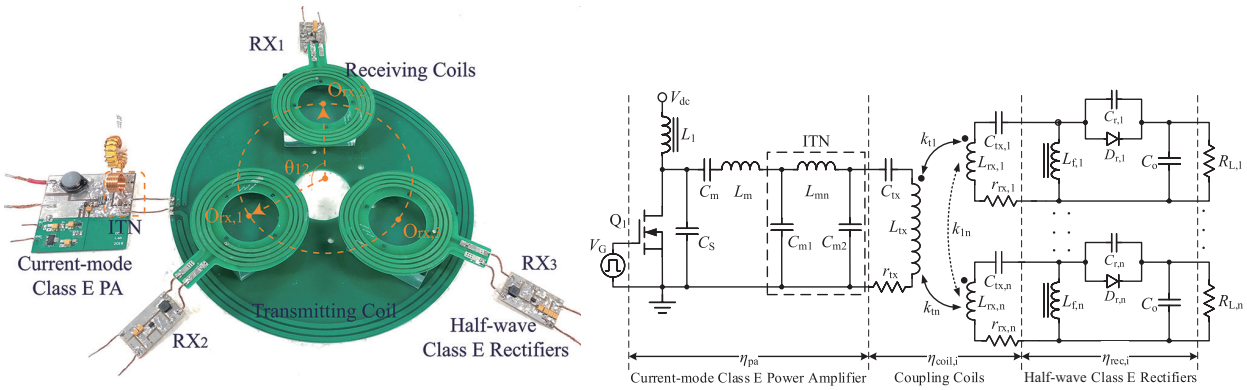

Fig. 13. A scalable multiple-receiver WPT system. (a) Experimental setup; (b) Circuit configuration.

Fig. 14 show the results using the conventional design, in which the influence of the cross coupling is neglected and the ITN is not included. This design obviously fails to decouple the power distribution among the receivers.

Fig. 15 shows the experimental results under varying cross coupling. First, the two receivers, RX_1 and RX_2, are placed with θ_{12}=180° position difference, i.e., a two-receiver system. Then RX_1 is moved along with the dashed circle illustrated in Fig. 13(a). The delivered load powers, $P_{RL,1}$ and $P_{RL,2}$, are measured versus the changing θ_{12}, namely the changing cross coupling. As shown in Fig. 15(a), with the above robust design, the target power distribution is well maintained over a wide range of θ_{12} from 180° to 100°. A high system efficiency η_{sys} (above 77%) and transmitting coil to load efficiency $\eta_{coil2load}$ are also observed [see Fig. 15(b)]. The results of the conventional design (dash lines) are co-listed in Fig. 15 for reference purposes.

V. Conclusions

Increasing the operating frequency to several MHz (such as 6.78 MHz) is particularly useful for improving the spatial freedom of the WPT and releasing additional design freedom. Meanwhile, because of the more obvious influence of the device parasitic parameters when operating at MHz, the system-level modeling and design are critical

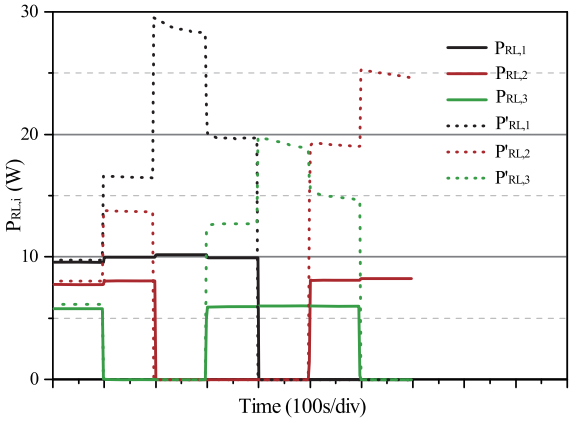

Fig. 14. Load powers with a changing combination of receivers.

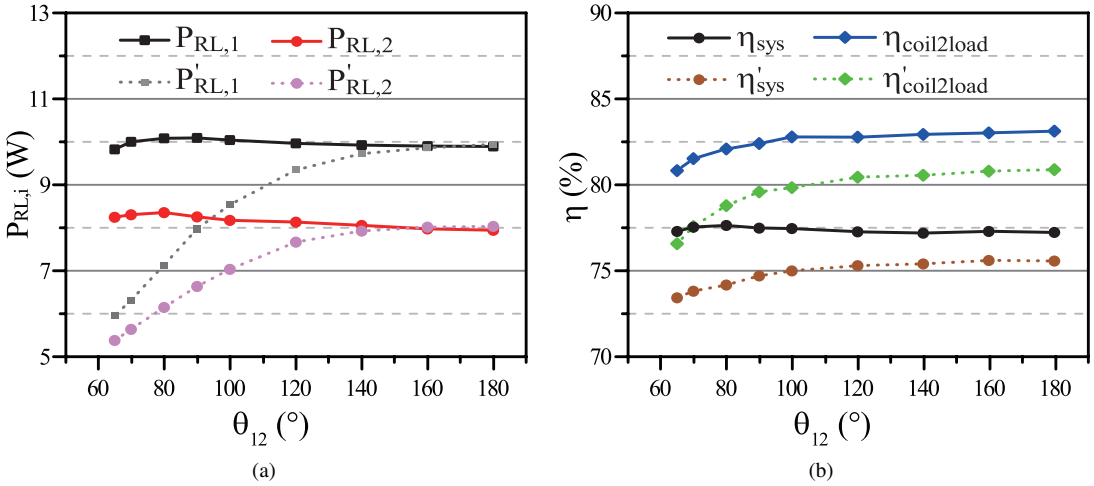

Fig. 15. Experimental results with varying cross coupling. (a) Load powers; (b) Efficiencies.

to improving the efficiency, EMI performance, and robustness of a final WPT system. This article begins with the typical power conversion circuit topologies and extends to the modeling and parameter design of a high-performance Class E^2 6.78 MHz WPT system. It also explains a robust design scheme dedicating to a multiple-receiver WPT system. The changing cross coupling between the receivers is explicitly reflected in the formulation of the design problem. Using the Class E rectifiers and the current-model Class E PA as supporting circuits, their parameters are optimized in a manner to maintain high system efficiency and target power distribution, when the cross coupling between the receivers varies within a certain range. As described in this article, developing high-performance MHz WPT systems will inevitably be a comprehensive effort involving interdisciplinary knowledge in device, circuitry, modeling, design and control.

ACKNOWLEDGEMENT

This work was partly supported by the Shanghai Natural Science Foundation (2016–2019) under the project "Research on Key Issues of Optimized Power Distribution in Multiple-Receiver Megahertz Wireless Power Transfer Systems" (grant 16ZR1416300).

BIOGRAPHIES

Ming Liu (ml45@princeton.edu) received the B.S. degree from Sichuan University, China, in 2007, and the Ph.D. degree in electrical and computer engineering from the University of Michigan-Shanghai Jiao Tong University Joint Institute, Shanghai Jiao Tong University, China, in 2017. He is currently a postdoctoral research fellow at Department of Electrical Engineering of Princeton University, Princeton, NJ, USA. His research interests include circuit topology and architecture, control strategy, and optimization-based design of megahertz wireless power transfer systems as well as high frequency power electronics. He was the recipient of the Research Excellence Award from AirFuel Alliance, USA, in 2019. He is a Member of the IEEE.

Zhang Huang (hzhang_93@sjtu.edu.cn) received the B.S. degree from Shandong University, China, in 2012, and the M.S. degree from Shanghai Jiao Tong University, China, in 2016. He is currently working toward the Ph.D. degree in electrical and computer engineering at the University of Michigan-Shanghai Jiao Tong University Joint Institute, Shanghai Jiao Tong University, China. His research interests include high frequency power electronics and its applications in compact and robust megahertz wireless power transfer systems. He is a Student Member of the IEEE.

Yaoxia Shao (yaoxiashao@sjtu.edu.cn) received the B.S. degree from Tongji University, China, in 2018. He is currently working toward the Ph.D. degree in electrical and computer engineering at the University of Michigan-Shanghai Jiao Tong University Joint Institute, Shanghai Jiao Tong University, China. His research interests include high-frequency power conversion circuits, and applications in both inductive power transfer and microwave power transfer. He is a student Member of the IEEE.

Jibin Song (jibinsong@sjtu.edu.cn) received the B.S. degree from Jilin University, China, in 2016. He is currently working toward the Ph.D. degree in electrical and computer engineering at University of Michigan-Shanghai Jiao Tong University Joint Institute, Shanghai Jiao Tong University, China. His research interests include modeling and design of multiple-receiver wireless power transfer systems and high-frequency high-efficiency power conversion circuits. He is a student Member of the IEEE.

Chengbin Ma (chbma@sjtu.edu.cn) received the B.S. degree from East China University of Science and Technology, China, in 1997, and the M.S. and Ph.D. degrees in electrical engineering from The University of Tokyo, Japan, in 2001 and 2004, respectively. From 2004 to 2006, he was an R&D Researcher with FANUC Limited, Japan. Between 2006 and 2008, he was a Postdoctoral Researcher with University of California, Davis, USA. He joined the University of Michigan-Shanghai Jiao Tong University Joint Institute, Shanghai Jiao Tong University, China, in 2008, and currently an Associate Professor of electrical and computer engineering. His research interests include megahertz wireless power transfer, energy management, dynamics and motion control, and wide applications in electronic devices, electric vehicles, microgrids, smart grids, etc. He was the recipient of the Research Excellence Award from AirFuel Alliance, USA, in 2019. He is a Senior Member of the IEEE.

REFERENCES

[1] A. M. Andwaria, A. Pesiridisa, S. Rajooc, R. Martinez-Botasd, and V. Esfahanianb, "A review of battery electric vehicle technology and readiness levels," *Renew. Sustain. Energy Rev.*, vol. 78, pp. 414–430, May 2017.

[2] F. Schlachter, "No moore's law for batteries," *Proc. Nat. Acad. Sci. USA*, vol. 110, no. 14, pp. 5273–5273, Apr. 2013.

[3] Z. Rezvani, J. Jansson, and J. Bodin, "Advances in consumer electric vehicle adoption research: A review and research agenda," *Transp. Res. D Transp. Environ.*, vol. 34, pp. 122–136, Jan. 2015.

[4] P. Albertus, G. Girishkumar, B. McCloskey, R. S. Sánchez-Carrera, B. Kozinsky, J. Christensen, and A. C. Luntz, "Identifying capacity limitations in the li/oxygen battery using experiments and modeling," *J. Electrochem. Soc.*, vol. 158, no. 3, pp. A343–A351, Jan. 2011.

[5] P. Albertus, S. Babinec, S. Litzelman, and A. Newman, "Status and challenges in enabling the lithium metal electrode for high-energy and low-cost rechargeable batteries," *Nat. Energy*, vol. 3, no. 1, pp. 16–21, Jan. 2018.

[6] N. Tesla, "The transmission of electrical energy without wires as a means for furthering peace," *Elect. World Eng.*, vol. 7, p. 21, Jan. 1905.

[7] D. Belo, D. C. Ribeiro, P. Pinho, and N. Borges Carvalho, "A selective, tracking, and power adaptive far-field wireless power transfer system," *IEEE Trans. Microw. Theory Tech.*, vol. 67, no. 9, pp. 3856–3866, Sep. 2019.

[8] K. Jin and W. Zhou, "Wireless laser power transmission: A review of recent progress," *IEEE Transactions on Power Electronics*, vol. 34, no. 4, pp. 3842–3859, Apr. 2019.

[9] F. Lu, H. Zhang, H. Hofmann, and C. Mi, "A double-sided LCLC-compensated capacitive power transfer system for electric vehicle charging," *IEEE Trans. Power Electron.*, vol. 30, no. 11, pp. 6011–6014, Nov. 2015.

[10] J. Dai and D. C. Ludois, "A survey of wireless power transfer and a critical comparison of inductive and capacitive coupling for small gap applications," *IEEE Trans. Power Electron.*, vol. 30, no. 11, pp. 6017–6029, Nov. 2015.

[11] A. Kurs, A. Karalis, R. Moffatt, J. D. Joannopoulos, P. Fisher, and M. Soljačić, "Wireless power transfer via strongly coupled magnetic resonances," *science*, vol. 317, no. 5834, pp. 83–86, Jul. 2007.

[12] "The Qi wireless power transfer system, power class 0 specification," *Wireless Power Consortium*, Apr. 2016, Available: https://www.wirelesspowerconsortium.com/.

[13] "Wireless power transfer for light-duty plug-in/electric vehicles and alignment methodology," *SAE International*, J2954, Apr. 2019.

[14] Z. Li, C. Zhu, J. Jiang, K. Song, and G. Wei, "A 3-kW wireless power transfer system for sightseeing car supercapacitor charge," *IEEE Trans. Power Electron.*, vol. 32, no. 5, pp. 3301–3316, May 2017.

[15] T. Kan, R. Mai, P. P. Mercier, and C. C. Mi, "Design and analysis of a three-phase wireless charging system for lightweight autonomous underwater vehicles," *IEEE Trans. Power Electron.*, vol. 33, no. 8, pp. 6622–6632, Aug. 2018.

[16] A. Zaheer, M. Neath, H. Z. Z. Beh, and G. A. Covic, "A dynamic EV charging system for slow moving traffic applications," *IEEE Trans. Transp. Electrif.*, vol. 3, no. 2, pp. 354–369, Jun. 2017.

[17] T. Diekhans and R. W. De Doncker, "A dual-side controlled inductive power transfer system optimized for large coupling factor variations and partial load," *IEEE Trans. Power Electron.*, vol. 30, no. 11, pp. 6320–6328, Nov. 2015.

[18] D. Ahn, S. Kim, J. Moon, and I.-K. Cho, "Wireless power transfer with automatic feedback control of load resistance transformation," *IEEE Trans. Power Electron.*, vol. 31, no. 11, pp. 7876–7886, Nov. 2016.

[19] A. Berger, M. Agostinelli, S. Vesti, J. A. Oliver, J. A. Cobos, and M. Huemer, "A wireless charging system applying phase-shift and amplitude control to maximize efficiency and extractable power," *IEEE Trans. Power Electron.*, vol. 30, no. 11, pp. 6338–6348, Nov. 2015.

[20] A. Zaheer, G. A. Covic, and D. Kacprzak, "A bipolar pad in a 10-kHz 300-W distributed IPT system for AGV applications," *IEEE Trans. Ind. Electron.*, vol. 61, no. 7, pp. 3288–3301, Jul. 2014.

[21] S. Kim, G. A. Covic, and J. T. Boys, "Tripolar pad for inductive power transfer systems for EV charging," *IEEE Trans. Power Electron.*, vol. 32, no. 7, pp. 5045–5057, Jul. 2017.

[22] "Airfuel resonant wireless power transfer (WPT) system baseline system specification (BSS)," *Alliance for Wireless Power*, 2014.

[23] S. Y. R. Hui, W. Zhong, and C. K. Lee, "A critical review of recent progress in mid-range wireless power transfer," *IEEE Trans. Power Electron.*, vol. 29, no. 9, pp. 4500–4511, Sep. 2014.

[24] R. Sector, "International telecommunication union (itu)," *General Aspects of Digital Transmission Systems–Terminal Equipments. Pulse Code Modulation of Voice Frequencies. ITU-T Recommendation G*, vol. 711, 2013.

[25] Z. Zhang, H. Pang, A. Georgiadis, and C. Cecati, "Wireless power transfer—an overview," *IEEE Trans. Ind. Electron.*, vol. 66, no. 2, pp. 1044–1058, Feb. 2019.

[26] K. Chen, Z. Zhao, L. Yuan, T. Lu, and F. He, "The impact of nonlinear junction capacitance on switching transient and its modeling for SiC MOSFET," *IEEE Trans. Electron Devices*, vol. 62, no. 2, pp. 333–338, Feb. 2015.

[27] T. Campi, S. Cruciani, V. De Santis, F. Palandrani, F. Maradei, and M. Feliziani, "Induced effects in a pacemaker equipped with a wireless power transfer charging system," *IEEE Trans. Magn.*, vol. 53, no. 6, pp. 1–4, Jun. 2017.

[28] C. Song, H. Kim, Y. Kim, D. Kim, S. Jeong, Y. Cho, S. Lee, S. Ahn, and J. Kim, "EMI reduction methods in wireless power transfer system for drone electrical charger using tightly coupled three-phase resonant magnetic field," *IEEE Trans. Ind. Electron.*, vol. 65, no. 9, pp. 6839–6849, Sep. 2018.

[29] P. C. Luk, S. Aldhaher, W. Fei, and J. F. Whidborne, "State-space modeling of a class E^2 converter for inductive links," *IEEE Trans. Power Electron.*, vol. 30, no. 6, pp. 3242–3251, Jun. 2015.

[30] K. Song, Z. Li, J. Jiang, and C. Zhu, "Constant current/voltage charging operation for series–series and series–parallel compensated wireless power transfer systems employing primary-side controller," *IEEE Trans. Power Electron.*, vol. 33, no. 9, pp. 8065–8080, Sep. 2018.

[31] S. Wang, J. Chen, Z. Hu, C. Rong, and M. Liu, "Optimisation design for series–series dynamic WPT system maintaining stable transfer power," *IET Power Electron.*, vol. 10, no. 9, pp. 987–995, Jul. 2017.

[32] H. Tebianian, Y. Salami, B. Jeyasurya, and J. E. Quaicoe, "A 13.56-MHz full-bridge class-D ZVS inverter with dynamic dead-time control for wireless power transfer systems," *IEEE Trans. Ind. Electron.*, vol. 67, no. 2, pp. 1487–1497, Feb. 2020.

[33] M. Liu, M. Fu, and C. Ma, "Low-harmonic-contents and high-efficiency class E full-wave current-driven rectifier for megahertz wireless power transfer systems," *IEEE Trans. Power Electron.*, vol. 32, no. 2, pp. 1198–1209, Feb. 2017.

[34] H. Tebianian, Y. Salami, B. Jeyasurya, and J. E. Quaicoe, "A 13.56-MHz full-bridge class-D ZVS inverter with dynamic dead-time control for wireless power transfer systems," *IEEE Trans. Ind. Electron.*, vol. 67, no. 2, pp. 1487–1497, Feb. 2020.

[35] N. O. Sokal and A. D. Sokal, "Class E-a new class of high-efficiency tuned single-ended switching power amplifiers," *IEEE J. Solid-State Circuits*, vol. 10, no. 3, pp. 168–176, Jun. 1975.

[36] M. K. Kazimierczuk, "Analysis of class E zero-voltage-switching rectifier," *IEEE Trans. Circuits Syst.*, vol. 37, no. 6, pp. 747–755, Jun. 1990.

[37] M. K. Kazimierczuk and D. Czarkowski, *Resonant power converters*. John Wiley & Sons, 2012.

[38] S. Liu, M. Liu, S. Yang, C. Ma, and X. Zhu, "A novel design methodology for high-efficiency current-mode and voltage-mode class-E power amplifiers in wireless power transfer systems," *IEEE Trans. Power Electron.*, vol. 32, no. 6, pp. 4514–4523, Jun. 2017.

[39] F. Chen, J. Chen, and R. Lin, "Low-harmonic push–pull class-E power amplifier with a pair of LC resonant networks," *IEEE Trans. Circuits Syst.*, vol. 54, no. 3, pp. 579–589, Mar. 2007.

[40] Z. Kaczmarczyk and W. Jurczak, "A push–pull class-E inverter with improved efficiency," *IEEE Trans. Ind. Electron.*, vol. 55, no. 4, pp. 1871–1874, Apr. 2008.

[41] A. Reatti, M. K. Kazimierczuk, and R. Redl, "Class E full-wave low dv/dt rectifier," *IEEE Trans. Circuits Syst.*, vol. 40, no. 2, pp. 73–85, Feb. 1993.

[42] J. M. Rivas, Y. Han, O. Leitermann, A. D. Sagneri, and D. J. Perreault, "A high-frequency resonant inverter topology with low-voltage stress," *IEEE Trans. Power Electron.*, vol. 23, no. 4, pp. 1759–1771, Jul. 2008.

[43] X. Qu, H. Han, S. Wong, C. K. Tse, and W. Chen, "Hybrid IPT topologies with constant current or constant voltage output for battery charging applications," *IEEE Trans. Power Electron.*, vol. 30, no. 11, pp. 6329–6337, Nov. 2015.

[44] "(2020) The AirFuel Alliance website. [online]. available: https://airfuel.org/."

[45] M. Liu, M. Fu, and C. Ma, "Parameter design for a 6.78-MHz wireless power transfer system based on analytical derivation of class E current-driven rectifier," *IEEE Trans. Power Electron.*, vol. 31, no. 6, pp. 4280–4291, Jun. 2016.

[46] A. Ivascu, M. K. Kazimierczuk, and S. Birca-Galateanu, "Class E resonant low dv/dt rectifier," *IEEE Trans. Circuits Syst.*, vol. 39, no. 8, pp. 604–613, Aug. 1992.

[47] M. Fu, Z. Tang, and C. Ma, "Analysis and optimized design of compensation capacitors for a megahertz WPT system using full-bridge rectifier," *IEEE Trans. Ind. Informat.*, vol. 15, no. 1, pp. 95–104, Jan. 2019.

[48] F. Raab, "Idealized operation of the class E tuned power amplifier," *IEEE Trans. Circuits Syst.*, vol. 24, no. 12, pp. 725–735, Dec. 1977.

[49] M. Albulet, *RF power amplifiers*. SciTech Publishing, 2001.

[50] M. H. Rashid, *Spice for power electronics and electric power*. CRC press, 2016.

[51] D. Ahn and S. Hong, "Effect of coupling between multiple transmitters or multiple receivers on wireless power transfer," *IEEE Trans. Ind. Electron.*, vol. 60, no. 7, pp. 2602–2613, Jul. 2013.

[52] F. Liu, Y. Yang, Z. Ding, X. Chen, and R. M. Kennel, "Eliminating cross interference between multiple receivers to achieve targeted power distribution for a multi-frequency multi-load mcr wpt system," *IET Power Electron.*, vol. 11, no. 8, pp. 1321–1328, Jun. 2018.

[53] F. Liu, Y. Yang, Z. Ding, X. Chen, and R. M. Kennel, "A multifrequency superposition methodology to achieve high efficiency and targeted power distribution for a multiload MCR WPT system," *IEEE Trans. Power Electron.*, vol. 33, no. 10, pp. 9005–9016, Oct. 2018.

[54] W. Zhong and S. Y. R. Hui, "Auxiliary circuits for power flow control in multifrequency wireless power transfer systems with multiple receivers," *IEEE Trans. Power Electron.*, vol. 30, no. 10, pp. 5902–5910, Oct. 2015.

[55] R. Narayanamoorthi, A. Vimala Juliet, and B. Chokkalingam, "Cross interference minimization and simultaneous wireless power transfer to multiple frequency loads using frequency bifurcation approach," *IEEE Trans. Power Electron.*, vol. 34, no. 11, pp. 10 898–10 909, Nov. 2019.

[56] Y. J. Kim, D. Ha, W. J. Chappell, and P. P. Irazoqui, "Selective wireless power transfer for smart power distribution in a miniature-sized multiple-receiver system," *IEEE Trans. Ind. Electron.*, vol. 63, no. 3, pp. 1853–1862, Mar. 2016.

[57] H. Yin, M. Fu, M. Liu, J. Song, and C. Ma, "Autonomous power control in a reconfigurable 6.78-MHz multiple-receiver wireless charging system," *IEEE Trans. Ind. Electron.*, vol. 65, no. 8, pp. 6177–6187, Aug. 2018.

[58] K. Lee and D. Cho, "Analysis of wireless power transfer for adjustable power distribution among multiple receivers," *IEEE Antennas Wireless Propag. Lett.*, vol. 14, pp. 950–953, Jan. 2015.

[59] J. Song, M. Liu, and C. Ma, "Analysis and design of a high-efficiency 6.78-MHz wireless power transfer system with scalable number of receivers," *IEEE Trans. Ind. Electron.*, DOI:10.1109/TIE.2019.2950850, 2019.

[60] G. Wei, X. Jin, C. Wang, J. Feng, C. Zhu, and M. I. Matveevich, "An automatic coil design method with modified ac resistance evaluation for achieving maximum coil–coil efficiency in wpt systems," *IEEE Trans. Power Electron.*, vol. 35, no. 6, pp. 6114–6126, Jun. 2020.

[61] T. Yilmaz, N. Hasan, R. Zane, and Z. Pantic, "Multi-objective optimization of circular magnetic couplers for wireless power transfer applications," *IEEE Trans. Magn.*, vol. 53, no. 8, pp. 1–12, Aug. 2017.